Applied Catalysis B: Environmental 178 (2015) 226–232

Contents lists available at ScienceDirect

Applied Catalysis B: Environmental

journal homepage: www.elsevier.com/locate/apcatb

Mixed-phase nanocrystalline TiO_2 photocatalysts produced by flame spray pyrolysis

Luca Giacomo Bettini[a,b], Maria Vittoria Dozzi[c], Flavio Della Foglia[a,b], Gian Luca Chiarello[c], Elena Selli[a,c,*], Cristina Lenardi[a,b], Paolo Piseri[a,b], Paolo Milani[a,b]

[a] CIMAINA,Università degli Studi di Milano, via Celoria 16, 20133 Milano, Italy
[b] Dipartimento di Fisica,Università degli Studi di Milano, via Celoria 16, 20133 Milano, Italy
[c] Dipartimento di Chimica, Università degli Studi di Milano, via Golgi 19, 20133 Milano, Italy

ARTICLE INFO

Article history:
Received 7 July 2014
Received in revised form 30 August 2014
Accepted 7 September 2014
Available online 16 September 2014

Keywords:
Titanium dioxide
Flame spray pyrolysis
Nanoparticles
Photocatalytic degradation
Formic acid

ABSTRACT

Titanium dioxide nanostructured powders with different structural properties and improved photocatalytic performance were synthesized by flame spray pyrolysis (FSP) under systematically varied FSP operation conditions, starting from organic solutions containing titanium(IV) isopropoxide (TTIP) as Ti precursor. The primary particle size, crystalline phase, specific surface area, porosity and morphology of the so obtained photocatalyst powders were investigated by means of Raman spectroscopy, XRD, BET, SEM and UV–vis absorption analysis. An increase of the molar ratio between the dispersion oxygen gas and the TTIP fed into the flame was demonstrated to lead to TiO_2 materials with decreased primary particles size, from ca. 21 to 7 nm, with a higher brookite content and an increased BET surface area, from ca. 70 up to 250 $m^2 g^{-1}$. The photocatalytic activity of the as-synthesized TiO_2 powders was investigated employing formic acid decomposition in aqueous suspension as test reaction. With the TiO_2 powders synthesized with high O_2/TTIP flux molar ratio a formic acid photomineralization rate was attained significantly overcoming that obtained with commercial P25 TiO_2.

1. Introduction

Cost effective, efficient and scalable conversion of solar radiation is a key challenge for a sustainable energy economy [1] that can be met through the design and synthesis of improved light harvesting materials [2]. To this purpose, high surface nanostructured metal oxide semiconductors have long been the object of research efforts for their ability to convert light into chemical energy through photocatalytic processes [3]. Among these materials, titanium dioxide, thanks to its high photocatalytic activity, non-toxicity and relatively low cost, is still at the forefront as the most studied one, therefore also being the closest one to find practical application. The ability to tailor its structural properties (e.g. morphology, structure, band gap) at the synthesis stage is pivotal toward its optimization in view of real technological applications [4].

Flame spray pyrolysis (FSP) processes are well known gas phase combustion synthesis methods, which are used to prepare a wide variety of metal oxides, such as SiO_2, TiO_2 and Al_2O_3, in the form of nanocrystalline powders with high surface area [5,6]. As these methods allow a precise control over the powder structural characteristics [5,7], they hold great potential toward the synthesis of nanostructured metal oxide photocatalysts with improved performances.

FSP processes are based on the exothermic combustion of a spray of an organic liquid precursor. By means of a suitable nozzle-equipped burner, a liquid-phase mixture containing a metallorganic compound and a solvent is dispersed into a flame where the resulting mixture droplets are combusted generating small clusters, which grow up by collisions and sintering processes taking place in the high temperature environment of the flame [5,8]. Due to the abundance of oxygen in the FSP reactor, which is typically provided both as dispersion and sheath gas, and to the high temperature of the flame, the nanoparticles produced by FSP are typically fully oxidized and crystalline. Therefore, no post-production heat treatment steps are required and the nanoparticles are immediately ready to use.

Although TiO_2 produced by FSP is an efficient photocatalyst for the photo-mineralization of several organic compounds [9] and its performance can be further improved by TiO_2 doping and/or loading with Au [10,11], V [12], Fe [13] and Pt [14] nanoparticles

* Corresponding author at: Dipartimento di Chimica, Università degli Studi di Milano, via Golgi 19, I-20133 Milano, Italy. Tel.: +39 02 503 14237; fax: +39 02 503 14300.
E-mail address: elena.selli@unimi.it (E. Selli).

http://dx.doi.org/10.1016/j.apcatb.2014.09.013
0926-3373/

directly during the FSP synthesis, its structural features and the resulting photocatalytic activity are critically affected by the FSP operation conditions, such as the oxygen partial pressure of the sheath environment [15], the combustion enthalpy of the organic solvent employed as fuel during the FSP synthesis [10] and the feed flow rate of the precursor solution [14]. A thorough investigation of the influence of the FSP process parameters over the TiO_2 structural properties is thus pivotal toward the effective, reliable and affordable FSP production of TiO_2-based photocatalysts.

Here, we present a systematic study of the effect of the synthesis parameters on the characteristics of TiO_2 powders produced by FSP. We show that the primary particle size, the relative abundance of the different crystalline phases (anatase, rutile and brookite) and the specific surface area of the powders are intimately related to the operation conditions of the synthesis process. The photocatalytic activity of the different FSP-made TiO_2 powders was tested in the photo-mineralization of formic acid (FA) in aqueous suspension and correlated to their structural properties and synthesis conditions.

2. Experimental

2.1. TiO_2 synthesis

TiO_2 nanostructured powders were produced in the gas-phase by the flame spray pyrolysis of titanium (IV) isopropoxide (TTIP, Aldrich, purity >97%) dissolved in two different organic solvents (i.e. ethanol and xylene), employing a commercial FSP system (NPS10, Tethis S.p.A., Italy). The TTIP precursor/solvent mixture was injected by a syringe pump through a stainless-steel capillary tube in a water-cooled nozzle, where it was dispersed into fine droplets by a coaxial gas flow of oxygen fed through an annular gap surrounding the capillary tube. The resulting spray was ignited by a pilot methane/oxygen flamelet (the flow rate of CH_4 and O_2 was 1.5 and 3 L min^{-1}, respectively), so that the organic part of the precursor solution was combusted, while the metal was oxidized and formed particles that grew by coagulation and sintering in the flame. The precursor liquid feed flow rate was measured by a mass rate controlled syringe pump, and all gas flows were adjusted by mass flow controllers. Different TiO_2 powders were produced varying the TTIP concentration in the precursor solution, the type of solvent and the feed flow rates of the precursor solution and of the dispersion and sheath gases, as reported in Table 1. The pressure drop of the dispersion O_2 gas at the nozzle tip was fixed at ca. 1.8 bar. The FSP-made powders were collected using a watercooled, stainless-steel filter housing supporting a glass microfiber filter (Whatman GF6, 257 mm in diameter), with exhaust gases drawn by a vacuum pump (Busch, Seco SV/SD 1010-1040C). The filter was located downstream the FSP reactor at distance of ca. 640 mm from the nozzle of the burner.

2.2. Structural characterization

X-ray powder diffraction (XRPD) patterns were recorded on a Philips PW3020 powder diffractometer, by using the Cu $K\alpha$ radiation (λ = 1.54056 Å). Quantitative phase analysis was made by the Rietveld refinement method [16], using the "Quanto" software. The average anatase crystallite size was calculated according to the Scherrer equation, from the integral XRD peak width calculated as the ratio between the peak area and peak intensity obtained by fitting with a Gaussian function the profile of the most intense reflections at $2\theta = 25.4^\circ$.

Raman spectra of the as-synthesized TiO_2 powders were recorded by an optical bench setup consisting in an Ar ion laser emitting at 514 nm (Spectra Physics, Beamlok series 2065-7) as excitation source, a single monochromator (ActonSP-2558-9N) equipped with a 1200 mm^{-1} blaze grating, a notch filter (RazorEdge® long wave pass filter LP02-514RE-25), and a liquid nitrogen-cooled CCD camera. Diffuse reflectance (R) spectra of the photocatalyst powders were recorded on a Jasco V-670 spectrophotometer equipped with a PIN-757 integrating sphere, using barium sulphate as a reference, and then converted into absorption (A) spectra ($A = 1 - R$).

The BET specific surface area (SSA) and pore-volume distribution were measured by N_2 adsorption/desorption at liquid nitrogen temperature in a Micromeritics Tristar II 3020 V1.03 apparatus, after out-gassing at 300 °C for 1 h under N_2 stream. Scanning electron microscopy (SEM) micrographs were acquired with a Zeiss ΣIGMA field emission instrument equipped with a Zeiss GEMINI electron optical column.

2.3. Photocatalytic tests

Photocatalytic FA degradation runs were performed under atmospheric conditions in a magnetically stirred 60 mL cylindrical quartz reactor, inserted in the already described [17,18] homemade housing consisting in a black box mounted on optical bench. All irradiated aqueous suspensions contained 0.1 g L^{-1} of photocatalyst and an initial FA concentration equal to 1.0×10^{-3} mol L^{-1}. After preliminary ultrasound treatment for 30 min, they were magnetically stirred in the dark for 15 min to attain the adsorption equilibrium of the substrate on the photocatalyst surface, before starting irradiation. Stirring was continued during the runs. At different time intervals, 2 mL-samples of the suspension were withdrawn from the reactor and centrifuged. The supernatant was analyzed for residual FA content by ion chromatography with conductivity detection, employing a Metrohm 761 Compact IC instrument, after calibration for formate ion concentration in the 0–50 ppm range. All kinetic runs were performed at natural pH, up to ca. 70% substrate degradation, and repeated at least twice, to check their reproducibility. During FA degradation the pH of the suspensions increased, from initial values around 3.7 to ca. 4.8, as a consequence of FA mineralization to CO_2 and H_2O.

Table 1
Synthesis parameters, phase composition (A = anatase, R = rutile), obtained from XRD analysis by assuming the absence of amorphous phase, anatase crystallites size, d_A, and specific surface area (SSA), calculated by BET isotherms, of the FSP-made TiO_2 photocatalysts.

Sample	Solvent	TTIP (M)	Precursor flow (mL min^{-1})	O_2 dispersion (L min^{-1})	O_2 sheath (L min^{-1})	A (wt%)	R (wt%)	d_A (nm)	SSA (m^2 g^{-1})
FSP1	Ethanol	0.45	4	5	0	86	14	10*	121
FSP2	Xylene	0.45	4	5	0	82	18	12	113
FSP3	Xylene	0.8	4	5	0	78	22	15	90
FSP4	Xylene	0.45	1	5	0	88	11	7	249
FSP5	Xylene	0.45	8	5	0	86	14	17	72
FSP6	Xylene	0.45	4	8	0	73	27	9	161
FSP7	Xylene	0.45	4	5	5	78	22	11	123

* Bimodal distribution of particle size: ca. 2/3 of FSP1 anatase particles have d_A = 10 nm, 1/3 of them has d_A around 50 nm.

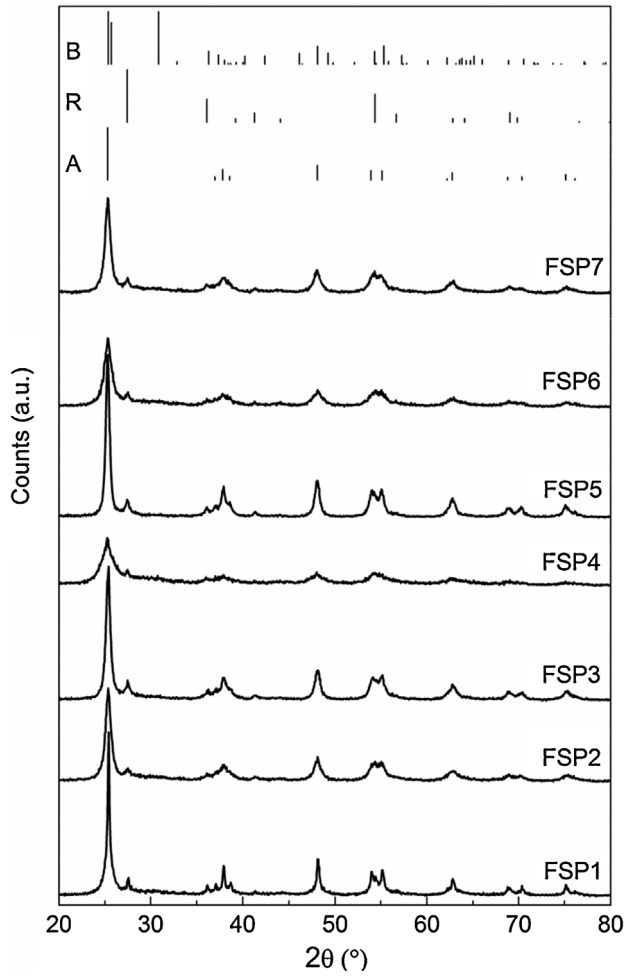

Fig. 1. XRD diffractograms of the as-synthesized FSP-made TiO_2 powders together with the position of the diffraction peaks of anatase (A), rutile (R) and brookite (B).

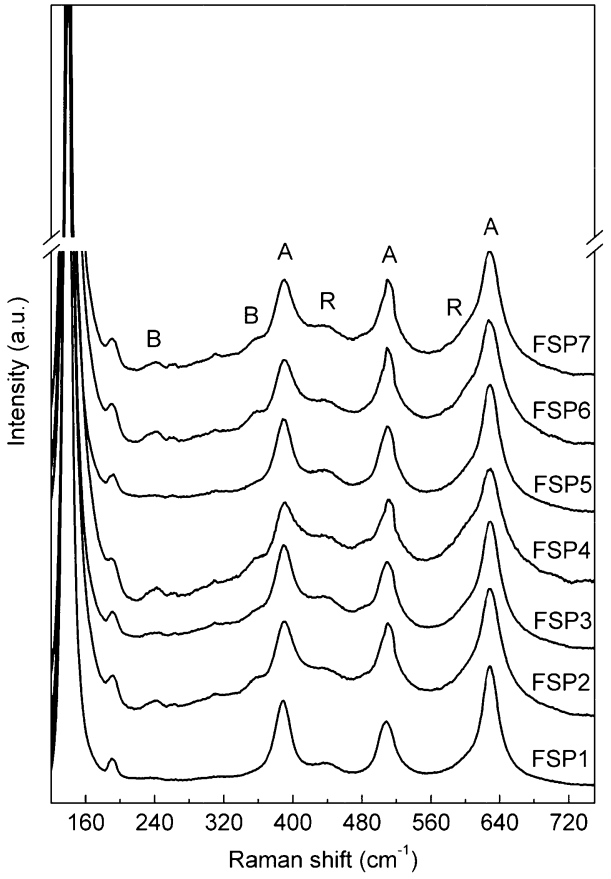

Fig. 2. Raman spectra of TiO_2 powders produced by FSP according to the operation parameters reported in Table 1.

3. Results and discussion

3.1. Photocatalyst characterization

Different TiO_2 nanostructured powders were produced by FSP according to the operation conditions (solvent, TTIP concentration, feed precursor solution, dispersion and sheath gas flow rates) reported in Table 1, which are expected to significantly modify the synthesis conditions in terms of flame temperature, nanoparticles concentration and residence time in the flame [7,10,14,15]. The XRD patterns of the FSP-made TiO_2 powders reported in Fig. 1 indicate that they contained a mixture of anatase and rutile phases. The overlap between the XRD peaks of anatase and brookite does not allow to ascertain the presence of this latter crystalline phase; the absence of a clear diffraction peak at $2\theta = 31^\circ$ suggests that brookite is not formed in a significant amount during the FSP process.

An XRD peak broadening with the trend FSP1 < FSP5 < FSP3 < FSP2 < FSP7 < FSP6 < FSP4 can be observed. As the width of the XRD peaks is related to the crystallite size of the material, this broadening indicates that the characteristics of the TiO_2 powders are affected by the FSP operation conditions. Anatase and rutile contents were calculated by the analysis of XRD diffractograms and reported in Table 1 together with the size of the anatase crystallites, which was the main crystalline phase (>70 wt%) in all samples.

XRD patterns indicate that a lower anatase content was obtained when xylene (FSP2) was used as solvent/fuel instead of ethanol (FSP1). Indeed, a higher combustion enthalpy (−1371 and −4552 kJ mol^{-1} for ethanol and xylene, respectively) is expected to lead to a higher flame temperature favoring the formation of the rutile phase. Furthermore, a bimodal anatase crystal size distribution was ascertained in the case of FSP1 by convoluting the XRP data into two superimposed modes, a major component, consisting in ca. 2/3 of the anatase particles, having a particle size of 10 nm, and a minor component (ca. 1/3) consisting of larger particles with ca. 50 nm size. Indeed, as demonstrated by Mädler and Pratsinis [19], in low combustion enthalpy solvents such as ethanol differently sized nanoparticles tend to form by both gas- and droplet-to-particle conversion.

An increased TTIP concentration in the precursor solution, e.g. from 0.45 (FSP2) to 0.8 M (FSP3), resulted in larger TiO_2 nanoparticles due to the increased number of Ti atoms and TiO_2 clusters in the flame. A similar effect was obtained for a fixed 0.45 M TTIP concentration by increasing the precursor feed ratio into the flame from 4 mL min^{-1} (FSP2) to 8 mL min^{-1} (FSP5) and, for the same reason, the opposite trend was observed when the precursor flux was decreased to 1 mL min^{-1} (FSP4). The crystallite size and anatase content decreased when additional oxygen was provided by increasing the dispersion gas flow rate (FSP6), while they remained almost unaltered when additional oxygen was fed into the FSP reactor as sheath gas (FSP7).

The Raman spectra of all FSP-made TiO_2 powders reported in Fig. 2 show both anatase (144, 197, 394, 513 and 635 cm^{-1}) and rutile (442 and 602 cm^{-1}) peaks [20], confirming the presence of mixed anatase/rutile phases. Moreover, the Raman spectra of FSP2, FSP4, FSP6 and FSP7 present two additional Raman peaks at 246 and 366 cm^{-1} which indicate the presence of brookite crystallites [21]. These Raman features are also observed with lower intensity in the

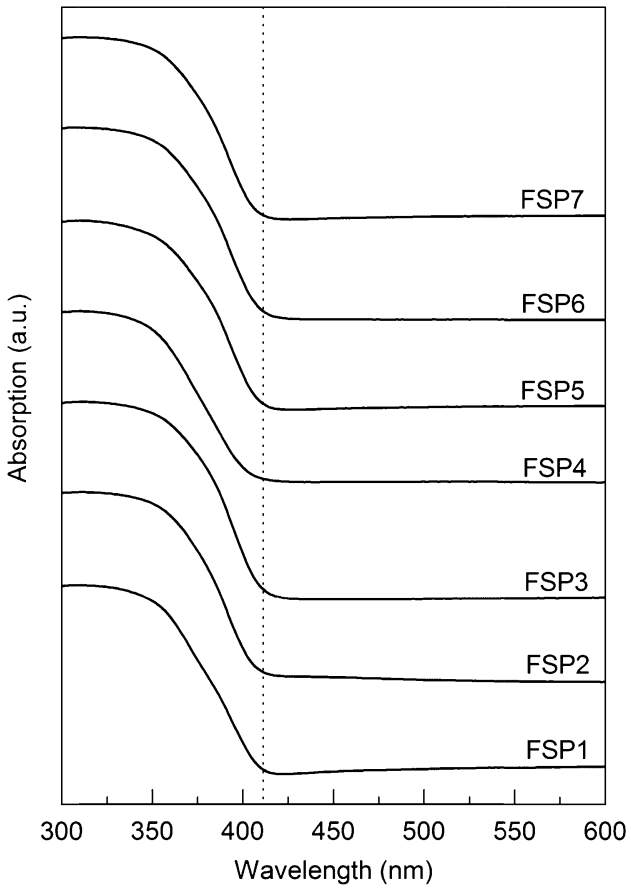

Fig. 3. UV–vis absorption spectra of the as-synthesized TiO_2 powders.

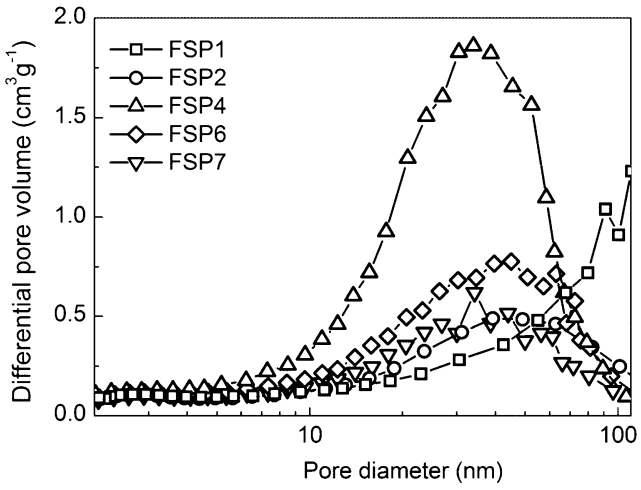

Fig. 4. Pore size distribution of FSP-made TiO_2 powders calculated by the BJH method.

Raman spectrum of FSP3. As the characteristic diffraction peak of brookite at $2\theta = 31^\circ$ was not detected in the XRD patterns of the FSP-made powders (Fig. 1), this TiO_2 crystalline phase is expected to be present in relatively small amounts, possibly below the detection limit of our XRD system (ca. 5%), and can be revealed by Raman spectroscopy thanks to the lack of overlap between the Raman signatures of the three different TiO_2 crystalline polymorphs. The Raman spectra indicate that the formation of the brookite phase is favored under the same synthesis conditions leading to anatase particles with size lower than 15 nm, while it is hampered in samples characterized by larger anatase crystallites (e.g. FSP1 and FSP5). This suggests that, as already reported in the case of TiO_2 nanocrystals prepared by the sol–gel method [22], the grain size plays a crucial role in determining both the phase stability and the phase transition sequence between anatase, brookite and rutile.

The UV–vis absorption spectra of the TiO_2 powders (see Fig. 3) show an absorption onset threshold located at ca. 410 nm consistent with the absorption edge of anatase and rutile phases. No marked differences were observed, as expected, between the absorption edges of the FSP-made powders and a band gap of 3.3 eV was evaluated by the Tauc method [23] for semiconductors with direct transition. Only FSP4 exhibits a slightly blue-shifted absorption onset due to a larger band gap of ca. 3.4 eV, which can be reasonably ascribed to the band gap widening due to the small size (quantum size effect) of anatase crystallites in this sample revealed by XRD analysis (see Table 1) [24].

Because of the aggregation and agglomeration of primary particles in the flame, FSP-made TiO_2 powders exhibit a porous structure which results in BET specific surface areas (SSA), determined by N_2 adsorption, ranging between 72 and 250 $m^2\,g^{-1}$ (Table 1). The SSA was slightly larger when ethanol (FSP1) instead of xylene (FSP2) was used as solvent/fuel in the synthesis, under otherwise identical conditions, and substantially increased when additional oxygen was fed into the flame as dispersion gas (FSP6). An increase in the precursor concentration (FSP3) and in the precursor flow rate (FSP5) resulted in lower SSA, which, oppositely, was significantly enhanced when the precursor feed flow rate was decreased (FSP4). The use of oxygen as sheath gas (FSP7) weakly affected the SSA.

The Barrett–Joyner–Halenda (BJH) analysis of the N_2 desorption isotherms shown in Fig. 4 reveals a macroporous structure of the FSP-made material obtained employing ethanol as a solvent/fuel. The structure of TiO_2 powders became mesoporous when the burner was fed with xylene solutions of the titanium precursor. A shift of the pore size distribution to narrower pore diameters with the trend FSP4 < FSP7 < FSP6 < FSP2 < FSP1 is observed. In particular, sample FSP4 exhibits a peculiar behavior, because of its smaller average pore size and much higher differential pore volume.

The scanning electron micrographs of selected FSP-made samples (Fig. 5) evidence a nanometric size of the TiO_2 primary particles and highlight the different powder morphologies arising from the change of the operation parameters in the synthesis. The use of xylene (FSP2) instead of ethanol (FSP1) seems to change the powder morphology toward a more accessible structure, which was further opened when the feed flow rate of the dispersion gas was increased (e.g. in FSP6). On the other hand, FSP4, though possessing the highest SSA, appears to be characterized by a more compact morphology at the micrometric scale.

The structural properties of the powders can be suitably related to the FSP operation conditions by describing these latter in terms of molar ratio φ (Eq. (1)) between the dispersion oxygen adopted in the synthesis and the TTIP amount fed into the flame, which was changed, in this work, over a wide range of values by setting different synthesis parameters (see Table 1).

$$\varphi = \frac{r_{O_2}}{r_{TTIP}} \tag{1}$$

Both r_{O_2} and r_{TTIP} are expressed in mol min^{-1}.

As shown in Fig. 6, whatever the operation conditions, the SSA of the FSP-made samples increased with increasing φ and the anatase crystallite size was in parallel drastically reduced. As the increase of oxygen concentration is expected to reduce the flame height, to decrease the droplet concentration of the spray flame and to produce a quenching effect owed to the additional gas that has to be heated by the same amount of fuel being burned [5,8,10,25,26], these findings can be ascribed to both a shorter residence time of

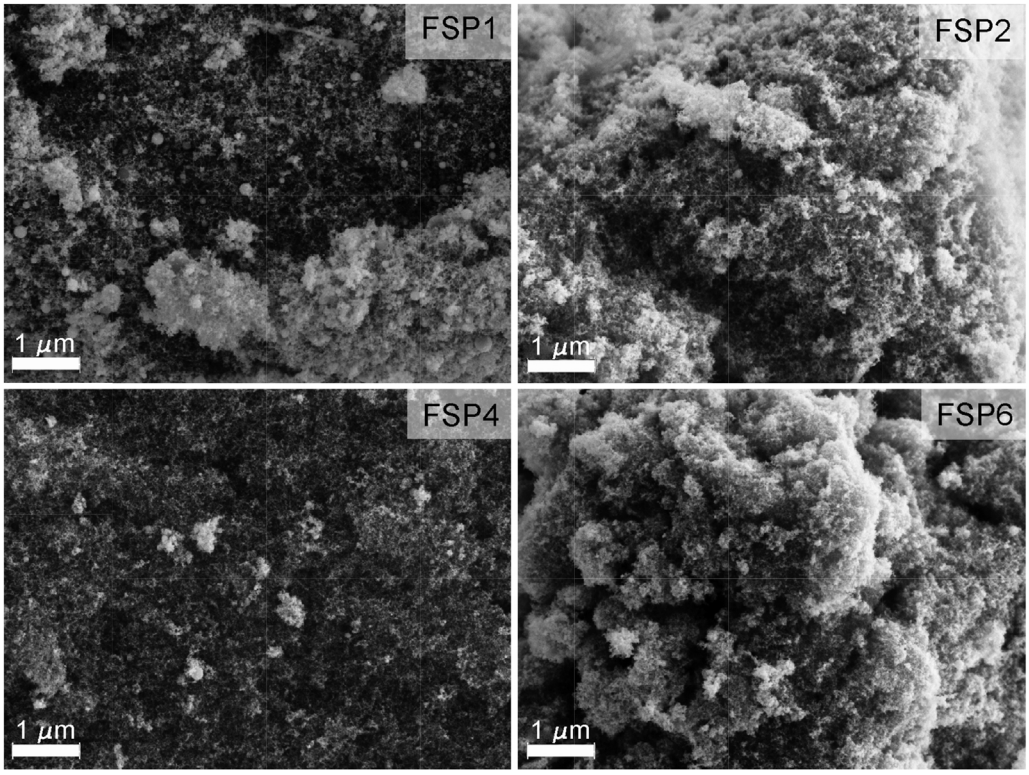

Fig. 5. SEM micrographs of FSP-made TiO_2 powders.

the particles in the flame and to a lower flame temperature, which reduce the time for crystallite growth and limit their sintering.

On the other hand, the introduction of additional oxygen as sheath gas in the FSP reactor (which is not taken into account when calculating φ) does not significantly affect the surface area and the size of the primary particles (see FSP7 vs. FSP2). Moreover, Fig. 6B shows that the size of the smaller anatase crystallite component of FSP1 perfectly fits the correlation obtained with all the other FSP-made materials.

Interestingly, as shown in Fig. 6A, the correlation existing between the SSA of the here investigated FSP-made TiO_2 samples and the φ parameter adopted in their synthesis (void symbols) holds also for different FSP-made TiO_2 powders synthesized by different research groups (full symbols) using xylene as solvent/fuel and oxygen as dispersion gas [10,13,27–31]. This highlights the pivotal role of the molar ratio between the dispersion oxygen and the titanium precursor fed into the burner in determining the powder properties and points to the φ parameter as a useful tool to tailor the properties of flame-made nanoparticles.

3.2. Photocatalytic tests

The oxidative photodegradation of formic acid in aqueous suspensions containing the FSP-made photocatalysts always occurred at constant rate, i.e. according to a zero-order rate law. The zero-order rate constants k^0 obtained in the runs carried out under identical conditions in the presence of the same amount (0.1 g L^{-1}) of the different photocatalyst powders are reported in Fig. 7 together with the k^0 value obtained under the same conditions employing TiO_2 P25 (Evonik), as standard commercial TiO_2 nanostructured powder photocatalyst.

As shown in Fig. 7, the photocatalytic activity of FSP1, obtained by employing ethanol as solvent/fuel in the FSP synthesis, was higher than that of FSP2 obtained employing xylene as solvent/fuel. Moreover, higher k^0 values were measured with photocatalyst samples produced starting from xylene solutions containing a fixed concentration of the titanium precursor, when the flux of precursor solution fed into the flame was increased (with the trend FSP4 < FSP2 <FSP5) and when a larger amount of oxygen was provided both as dispersion (FSP6) and as sheath gas (FSP7) (see Table 1). An increase in the TTIP concentration in the precursor solution produced powders ensuring a lower FA photo-mineralization rate (FSP3).

With the exception of samples FSP3 and FSP4, FA degradation rates measured with the FSP-made TiO_2 were comparable (FSP2 and FSP5) or significantly higher (FSP1, FSP6 and FSP7) than that obtained with P25 TiO_2. Moreover, the rate constant values reported in Fig. 7 indicate that the FSP-made TiO_2 powders produced in this work are better photocatalysts for FA photo-oxidation than pure TiO_2 powders prepared by the sol–gel method [18,32,33]. This demonstrates that highly active nanocrystalline TiO_2 photocatalysts can be synthesized by the FSP process under optimized operation conditions.

As for the structural characteristics, no clear correlation could be found between the k^0 values obtained with the different photocatalysts and their SSA, particles size or φ parameter. This means that the TiO_2 ability to initiate a surface reaction is not univocally determined by its surface area or strictly physical features, but it results from the synergistic effect of several physico-chemical properties, including the presence of not totally combusted carbonaceous species in the FSP-made materials and the presence of surface oxygen defects, depending on the flame conditions and residence time within the flame.

Although a beneficial effect of an increase of the dispersion oxygen concentration in the FSP reactor toward the FA photo-mineralization is highlighted by comparing the photocatalytic activity of samples FSP3, FSP2 and FSP6, the very low photocatalytic performance of FSP4 suggests that increasing φ above a critical value, besides producing powders with ultra-fine primary particles size and thus high SSA (see Table 1), is detrimental for the

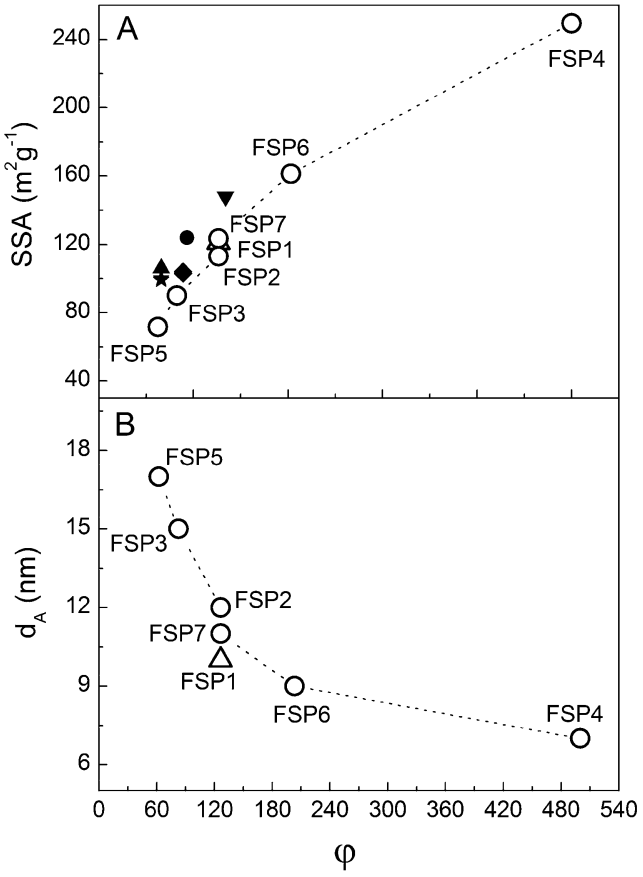

Fig. 6. (A) Specific surface area and (B) anatase crystallites size d_A vs. φ (Eq. (1)) of the here investigated TiO_2 samples (Table 1, void symbols) and of other FSP-made TiO_2 samples (full symbols): ⋆ Refs. [13,30]; ▲ Ref. [10]; ♦ Refs. [27,28]; ▼ Ref. [29]; ● Ref. [31].

photocatalytic activity of the TiO_2 powders. This is probably due to the low crystallinity of the so obtained material (see Fig. 1) and also to the small size of the produced anatase crystals (Table 1), evidencing quantum size effects with a blue shift of the light absorption threshold. On the other hand, a too small crystallite size also favors electron–hole recombination processes, hampering the photoinduced electron transfer between FA and TiO_2.

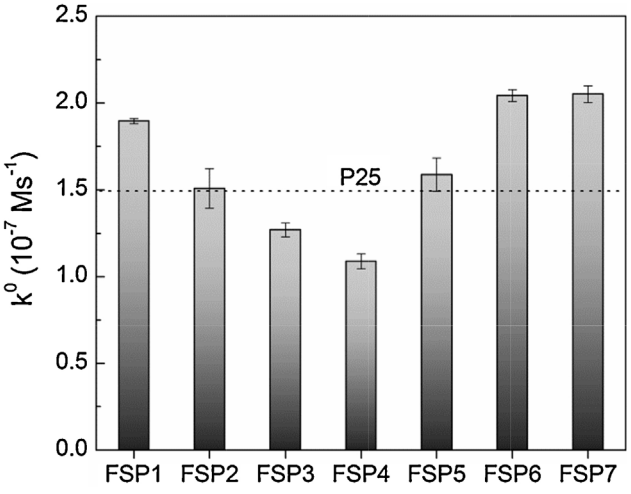

Fig. 7. Zero-order rate constants of FA photo-mineralization with FSP-made TiO_2 powders, in comparison with that obtained employing commercial P25 TiO_2 (dotted line).

Moreover, very different k^0 values were obtained with FSP1, FSP2 and FSP7, albeit featuring almost the same φ value. In the case of FSP1 and FSP2 this may be explained by structural differences due to the different solvent/fuel employed in the synthesis. In fact, FSP1 exhibits larger pores (see Fig. 4) and this macroporosity, if not significantly altered by the ultrasound treatment employed for the dispersion of the TiO_2 powder in water, may be beneficial in the photocatalytic degradation of the here investigated substrate. Conversely, the different photocatalytic activity of FSP7 and FSP2, possessing slightly different SSA and anatase/rutile composition but similar pore size distribution and crystallite size, may result from differences in the TiO_2 surface functional groups due to the presence of sheath O_2 during the synthesis of FSP7. Moreover, a higher brookite signal was obtained in the Raman spectra of FSP7 (Fig. 2), when the sheath gas was used. Mixtures of brookite with both anatase and rutile are known to be highly photoactive because of the presence of junctions among different polymorphic TiO_2 phases that enhance the separation of the photogenerated electron–hole pairs [34]. Furthermore, brookite crystals, compared to anatase crystals, were also reported to better adsorb FA [35], making this TiO_2 crystalline phase particularly promising for the photo-oxidation processes considered in this work.

4. Conclusions

The FSP technique demonstrates to allow the synthesis of TiO_2 photocatalyst powders with finely tuned properties. The morphology, crystal phase, primary particle size, specific surface area, porosity and photocatalytic activity of the materials strongly depend on FSP synthesis conditions, such as the solvent and the precursor concentration in the solutions fed into the burner and the precursor, dispersion and sheath gases flow rates. In particular, the molar ratio between the dispersion oxygen and the titanium precursor fed into the burner was found to be a suitable control parameter allowing one to finely tune the structural properties of FSP-made TiO_2 materials. The photocatalytic activity in formic acid photo-mineralization of the best performing flame-made TiO_2 photocatalyst powders, produced with a high feed flow rate of both dispersion and sheath oxygen, significantly overcomes that of commercial P25 TiO_2.

Acknowledgments

The authors thank Mariangela Longhi for BET measurements, Davide Marchesi for scanning electron microscopy analysis and Chiara Bigi for assistance in sample preparation. This work was supported by the Italian Ministry of University and Research (MIUR) “National Funding for Basic Research” (FIRB RBAP11AYN) project entitled “Oxides at the nanoscale: functionalities and applications”.

References

[1] J. Baxter, Z. Bian, G. Chen, D. Danielson, M.S. Dresselhaus, A.G. Fedorov, T.S. Fisher, C.W. Jones, E. Maginn, U. Kortshagen, A. Manthiram, A. Nozik, D.R. Rolison, T. Sands, L. Shi, D. Sholl, Y. Wu, Energy Environ. Sci. 2 (2009) 559–588.
[2] H. Tong, S. Ouyang, Y. Bi, N. Umezawa, M. Oshikiri, J. Ye, Adv. Mater. 24 (2011) 229–251.
[3] R. van de Krol, Y. Liang, J. Schoonman, J. Mater. Chem. 18 (2008) 2311–2320.
[4] K. Hashimoto, H. Irie, A. Fujishima, Jpn. J. Appl. Phys. 44 (2005) 8269–8285.
[5] W.Y. Teoh, R. Amal, L. Mädler, Nanoscale 2 (2010) 1324–1347.
[6] P. Roth, Proc. Combust. Inst. 31 (2007) 1773–1788.
[7] L. Mädler, H.K. Kammler, R. Mueller, S.E. Pratsinis, J. Aerosol Sci. 33 (2002) 369–389.
[8] R. Strobel, S.E. Pratsinis, J. Mater. Chem. 17 (2007) 4743–4756.
[9] W.Y. Teoh, F. Denny, R. Amal, D. Friedmann, L. Mädler, S.E. Pratsinis, Top. Catal. 44 (2007) 489–497.
[10] G.L. Chiarello, E. Selli, L. Forni, Appl. Catal., B: Environ. 84 (2008) 332–339.
[11] G.L. Chiarello, L. Forni, E. Selli, Catal. Today 144 (2009) 69–74.
[12] B. Tian, C. Li, F. Gu, H. Jiang, Y. Hu, J. Zhang, *Chem. Eng. J.* (2009) 220–227.
[13] W.Y. Teoh, R. Amal, L. Mädler, S.E. Pratsinis, Catal. Today 120 (2007) 203–213.

[14] W.Y. Teoh, L. Mädler, D. Beydoun, S.E. Pratsinis, R. Amal, Chem. Eng. Sci. 60 (2005) 5852–5861.
[15] Y.K. Kho, A. Iwase, W.Y. Teoh, L. Mädler, A. Kudo, R. Amal, J. Phys. Chem. C 114 (2010) 2821–2829.
[16] H.M. Rietveld, J. Appl. Cryst. 2 (1969) 65–71.
[17] M.V. Dozzi, L. Prati, P. Canton, E. Selli, Phys. Chem. Chem. Phys. 11 (2009) 7171–7180.
[18] M.V. Dozzi, S. Livraghi, E. Giamello, E. Selli, Photochem. Photobiol. Sci. 10 (2011) 343–349.
[19] L. Mädler, S.E. Pratsinis, J. Am. Ceram. Soc. 85 (2002) 1713–1718.
[20] A. Li Bassi, D. Cattaneo, V. Russo, C.E. Bottani, E. Barborini, T. Mazza, P. Piseri, P. Milani, F.O. Ernst, K. Wegner, S.E. Pratsinis, J. Appl. Phys. 98 (2005) 074305–74309.
[21] Y.H. Zhang, C.K. Chan, J.F. Porter, W. Guo, J. Mater. Res. 13 (1998) 2602–2609.
[22] K.R. Zhu, M.S. Zhanga, J.M. Honga, Z. Yin, Mater. Sci. Eng. A 403 (2005) 87–93.
[23] J. Tauc, Mater. Res. Bull. 5 (1970) 721–729.
[24] C. Kormann, D.W. Bahnemann, M.R. Hoffmann, J. Phys. Chem. 92 (1988) 5196–5201.
[25] R. Mueller, L. Mädler, S.E. Pratsinis, Chem. Eng. Sci. 58 (2003) 1969–1976.
[26] G.L. Chiarello, I. Rossetti, L. Forni, J. Catal. 236 (2005) 251–261.
[27] A. Tricoli, M. Righettoni, S.E. Pratsinis, Nanotechnology 20 (2009) 315502.
[28] A. Teleki, N. Bjelobrk, S.E. Pratsinis, Sens. Actuators, B: Chem. 130 (2008) 449–457.
[29] T. Rudin, K. Tsougeni, E. Gogolides, S.E. Pratsinis, Microelectron. Eng. 97 (2012) 341–344.
[30] L. Mädler, W. Stark, S.E. Pratsinis, J. Mater. Res. 18 (2003) 115–120.
[31] G.L. Chiarello, M.V. Dozzi, M. Scavini, J.D. Grunwaldt, E. Selli, App. Catal., B: Environ. 160–161 (2014) 144–151.
[32] M.V. Dozzi, B. Ohtani, E. Selli, Phys. Chem. Chem. Phys. 13 (2011) 18217–18227.
[33] M.V. Dozzi, A. Saccomanni, M. Altomare, E. Selli, Photochem. Photobiol. Sci. 12 (2013) 595–601.
[34] A. Di Paola, M. Bellardita, L. Palmisano, Catalysts 3 (2013) 36–73.
[35] W.K. Li, X.Q. Gong, G. Lu, A. Selloni, J. Phys. Chem. C 112 (2008) 6594–6596.